PTEP

Prog. Theor. Exp. Phys. **2015**, 073H01 (12 pages)
DOI: 10.1093/ptep/ptv096

A telescope proton recoil spectrometer for fast neutron beam-lines

C. Cazzaniga[1,3,*], M. Rebai[2,3], M. Tardocchi[3], G. Croci[2,3], M. Nocente[2,3], S. Ansell[1], C. D. Frost[1], and G. Gorini[2,3]

[1]*ISIS Facility, Science and Technology Facilities Council, Rutherford Appleton Laboratory, Didcot OX11 0QX, UK*
[2]*Università degli Studi di Milano-Bicocca, Dipartimento di Fisica, Piazza della Scienza 3, Milano, Italy*
[3]*Istituto di Fisica del Plasma "P. Caldirola", Associazione EURATOM-ENEA/CNR, Via Cozzi 53, Milano, Italy*
*E-mail: carlo.cazzaniga@mib.infn.it

Received September 29, 2014; Revised June 4, 2015; Accepted June 5, 2015; Published July 22, 2015

Fast neutron measurements were performed on the VESUVIO beam-line at the ISIS spallation source using a new telescope proton recoil spectrometer. Neutrons interact on a plastic target. Proton production is mainly due to elastic scattering on hydrogen nuclei and secondly due to interaction with carbon nuclei. Recoil protons are measured by a proton spectrometer, which uses in coincidence a 2.54 cm thick YAP scintillator and a 500 μm thick silicon detector, measuring the full proton recoil energy and the partial deposited energy in transmission, respectively. Recoil proton spectroscopy measurements (up to $E_p = 60$ MeV) have been interpreted by using Monte Carlo simulations of the beam-line. This instrument is of particular interest for the characterization of the ChipIr beam-line at ISIS, which was designed to feature an atmospheric-like neutron spectrum for the irradiation of micro-electronics.

Subject Index H10

1. Introduction

The new beam-line ChipIr has been built at the ISIS neutron source of the Rutherford Appleton Laboratory (UK) [1] for neutron irradiation experiments on electronic and avionic devices and systems. ChipIr is designed to feature a fast-neutron spectrum that mimics the atmospheric one with approximately 10^8–10^9 times higher intensity at ground level and approximately 300 times lower at normal flight altitude [2]. Atmospheric radiation is a major concern to the reliability of micro-electronic devices, which, due to their constantly decreasing dimensions and increased functionality, are more susceptible to failures caused by single-event effects (SEE) [3–5]. Because of their intense flux and high linear energy transfer, in the terrestrial environment neutrons represent the most important part of cosmic radiation producing single-event upsets [6].

The VESUVIO beam-line at ISIS, featuring a 300 K water moderator, was designed to have an under-moderated spectrum for studies in the eV energy range. Spallation neutrons, before the moderators, have a wide energy spectrum, ending at the energy of the proton beam (800 MeV). This configuration provides VESUVIO with an intense tail of fast neutrons ($5 \cdot 10^4$ neutrons cm^{-2} s^{-1} with $E_n > 10$ MeV), which has been exploited in recent years for the irradiation of micro-electronics [7–10].

The neutron energy spectrum and the flux spatial distribution of fast-neutron beam-lines (e.g. ChipIr and VESUVIO) are determined on the basis of Monte Carlo calculations that try to reproduce the complexity of nuclear and intra-nuclear interactions up to 800 MeV. Direct measurements of these quantities are needed for the characterization of the neutron flux, to benchmark the simulations, and for a better understanding of the underlying physics of this kind of facility.

Different kinds of fast-neutron detectors have been used to measure the fast-neutron flux [7,9,10] and several have been proposed for fast-neutron ($E_n > 10$ MeV) flux monitoring and imaging, such as diamond detectors [11–16] and gas detectors (nGEM) [17–20]. The threshold energy for the fast neutrons of interest for SEE studies is commonly taken to be 10 MeV, under the assumption that the contribution of lower-energy neutrons to the event rate is small [21]. A telescope proton recoil spectrometer (TPR) was developed for measurement of the fast-neutron spectrum with particular interest in the energy range 10 MeV $< E_n <$ 120 MeV, where SEE are manifested for most systems [21]. We here present measurements of recoil protons in the range 15 MeV $< E_p <$ 60 MeV, which, as shown below by Monte Carlo simulations, are mainly due to neutrons in the 30 MeV $< E_n <$ 120 MeV range. We do not address the contribution of lower-energy neutrons, i.e. the 10 MeV $< E_n <$ 30 MeV range, leaving this for future work.

The TPR system is composed of a thin plastic foil to convert neutrons into recoil protons and a high-resolution proton spectrometer.

A prototype TPR spectrometer was first tested on the VESUVIO beam-line, and the results were reported in Ref. [22]. In those preliminary measurements, a lithium glass scintillator was used for the transmission measurements (ΔE measurement), together with a 2.54 cm thick YAP crystal for the proton spectrometer (E measurement) [22].

As a further development, the lithium glass scintillator has been replaced by a silicon detector for ΔE measurements. This solution allows for better background discrimination due to a better energy resolution on the ΔE and fast signals. In this paper, the measurements performed with the TPR spectrometer using this detector configuration on the VESUVIO beam-line are reported. The interpretation of the measurements has been done using Monte Carlo simulations.

2. Experimental setup

A TPR neutron spectrometer is composed of a hydrogenated target, to convert neutrons into protons via elastic scattering, and a proton spectrometer. A picture of the experimental setup of the TPR spectrometer on the VESUVIO beam-line is shown in Fig. 1. A 2 mm thick polyethylene foil intercepts the entire beam cross section (about 5 cm in diameter). The proton spectrometer is placed clear of the neutron beam at 19 cm from the target and at an angle of 45° with respect to the neutron direction. At this angle, recoil protons have half of the corresponding neutron energy, due to the elastic scattering kinematics.

The efficiency and energy resolution of the TPR system depend on several parameters that have to be optimized; the most relevant effects are the contribution of the target thickness and the kinematic smearing effect due to the finite solid angle of the telescope and the finite size of the neutron-beam profile at the polyethylene converter. For a complete discussion, we refer to Ref. [22], where the calculations of efficiency and energy resolution for this geometry are presented. In the 30 MeV $< E_n <$ 120 MeV range, an acceptable efficiency level (ranging from $7 \cdot 10^{-6}$ to $4 \cdot 10^{-6}$) was obtained at the price of relatively poor energy resolution (ranging from 40% to 30%).

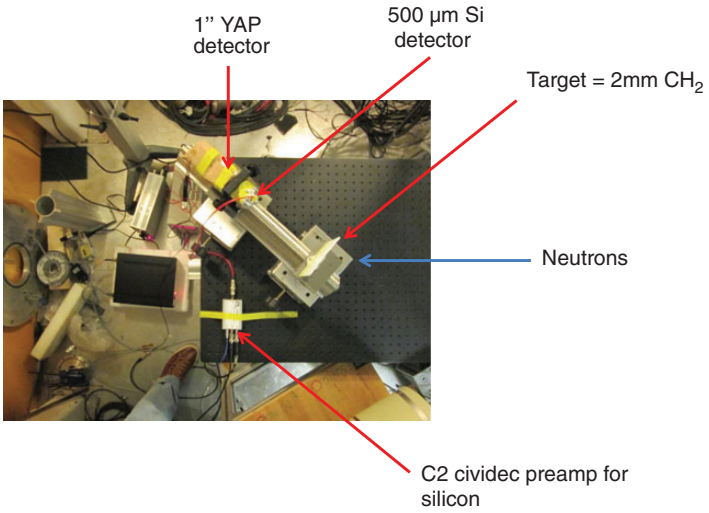

Fig. 1. Picture of the experimental setup of a TPR spectrometer on the VESUVIO beam-line of the ISIS spallation source.

The efficiency for neutrons in the 30 MeV $< E_n <$ 120 MeV range is dominated by the elastic scattering macroscopic cross section. A review of the world database on *np* scattering differential cross-section data up to 1000 MeV incident neutron energy can be found in Ref. [23].

In this configuration of the TPR, the proton spectrometer is composed of a 500 μm thick silicon detector for ΔE measurements and a 2.54 cm thick YAP scintillator for E measurements. The YAP scintillator is thick enough to stop protons up to about 100 MeV [24]. Both detectors have a circular section with a diameter of 2.54 cm. The YAP crystal is coupled to a Hamamatsu R9420-100-10mod photomultiplier tube (PMT) [25], where a high voltage (HV) of −600 V is applied. The silicon detector is coupled to a current preamplifier CIVIDEC C2 [26] with an HV of +170 V.

The YAP spectrometer was previously calibrated with gamma sources of ^{137}Cs and ^{60}Co. The ratio between the proton light yield to photon light yield is assumed to be 90% according to measurements performed at proton accelerators ([27,28] and [E. Perelli Cippo et al., in preparation]). The silicon spectrometer was calibrated using a ^{241}Am alpha source and with protons from 10 to 20 MeV at the Legnaro tandem accelerator [E. Perelli Cippo et al., in preparation].

Signals from the two detectors are fed into a 4 channel desktop digitizer with 1 GHz sampling frequency, 0–1 V input range and 10 bit resolution [29]. Since, at the ISIS neutron source, the beam is pulsed with a repetition frequency of 50 Hz, the board trigger is set on a reference signal (T_0) generated by the proton extraction from the synchrotron. For each T_0, a 3000 ns long waveform is stored for both detectors. Neutrons with $E_n >$ 10 MeV fall inside this short time window. Figure 2 shows an example of the two detector pulses recorded for the same T_0. The zero of the time scale is defined as the rising edge of the T_0 signal. Neutrons with $E_n >$ 10 MeV are recorded into the "pre-trigger" (i.e. negative time in the figure), because they arrive before the T_0 signal. This is due to the electronics used to extract the T_0 signal at ISIS and it is suitable for most of the instruments that work with a time of flight (ToF) in the ms time scale.

Due to the pulsed nature of the source, even if the global count rate is relatively low (the machine operates at 50 Hz), the instantaneous count rate is typically very high (>1 MHz), more than one signal pulse is typically present within a 1 μs window, and pile-up is an important issue. A fast scintillation time (27 ns for the YAP crystal), a dedicated voltage divider, and analysis algorithms are needed to cope with the high count rate, keeping a good energy resolution [30–33]. The coincidence analysis is

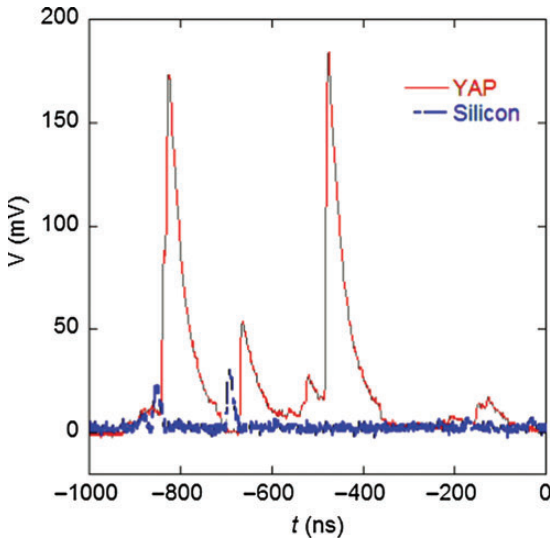

Fig. 2. Example of signal pulses from the two detectors composing the TPR. The signal of the YAP is recorded directly after the PMT, while the silicon signal is recorded after a current preamplifier.

carried out *offline* and includes pulse height (PH) and ToF spectral analysis. In the example of Fig. 2, one can notice three E signals with PH >50 mV ($t = -825$, -663, and -475 ns). Only the first two of these three have a corresponding ΔE signal from the silicon detector, and can be associated with a recoil proton event.

3. Optimization of $\Delta E - E$ coincidence of TPR measurements

A proton recoil spectrometer could, in principle, use a single detector. Multiple detectors are used in coincidence to reduce the background of secondary particles induced by fast neutrons (i.e. γ-rays and charged particles) [34–38]. The coincidence analysis of the TPR was optimized offline. Two events, E and ΔE, are considered to be in coincidence if the time difference Δt of their maxima falls inside a selected Δt window. Any rising edge in the waveform with amplitude above a *user-defined* threshold is defined as an *event*. In order to reduce the probability of random coincidences, the Δt window must be set as short as possible. The Δt window is not centered to zero, since different time delays are introduced by the PMT and the preamplifier. The center of the Δt window was found using a routine that counts the number of coincidence events as a function of Δt. The result is plotted in Fig. 3. True coincidence events appear in a peak, which rises over a continuum of random coincidences. According to these results, the Δt window was centered at -27.5 ns with a 10 ns width.

A further tool for data reduction is given by the relation between E and ΔE. Figure 4 shows the ΔE–E contour plot of coincidence events measured by the TPR. Proton-related events have a characteristic distribution due to the *Bethe formula* [39]. Energy thresholds are defined accordingly; the threshold on E is 8 MeV, which is the minimum energy for a proton to be transmitted by silicon. The threshold on ΔE is set above the electronic noise. Protons can be measured up to 60 MeV with this system. Above this value, the ΔE signal is too small (PH is less than 10 mV).

4. Measured proton spectra

The results of the ToF and PH coincidence analysis are presented in Figs. 5 and 6, respectively. A measurement without the scattering target ("no target" in Figs. 5 and 6) was carried out to estimate the background level; it is shown for comparison normalized to the integrated beam current.

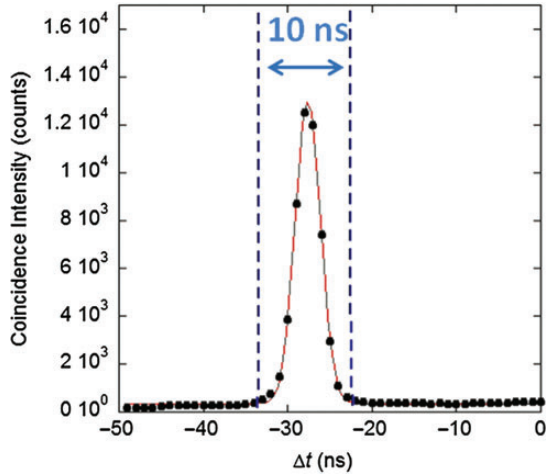

Fig. 3. Coincidence events as a function of the time difference of YAP and Si events (E and ΔE). True coincidence events appear in a peak, which rises over a continuum of random coincidences. The continuous line is a Gaussian fit of the data. Dashed lines indicate the limit of the Δt window selected for the TPR measurements.

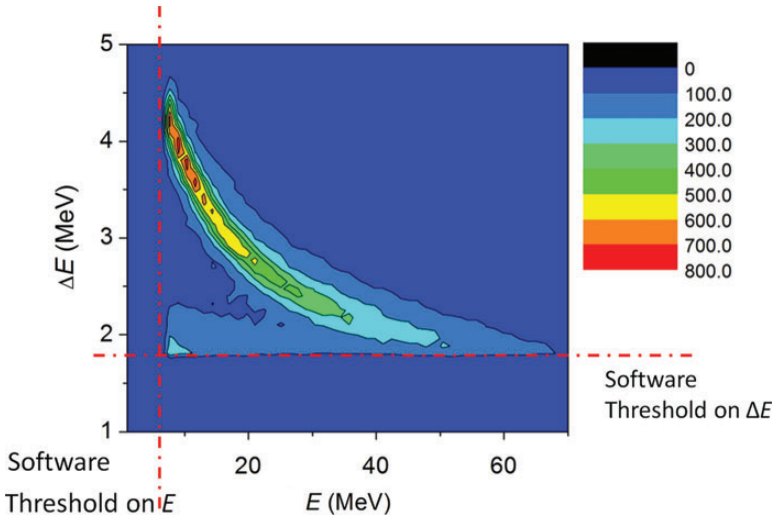

Fig. 4. ΔE–E contour plot of coincidence events measured by the TPR. The chromatic scale indicates the count intensity. Dashed lines indicate the software energy threshold used for the offline analysis.

The time distribution of the coincidence counts reflects the double-bunch structure of the ISIS proton beam. Every proton bunch is 70 ns wide and, for this reason, neutron spectroscopy in the MeV range or above is impossible with ToF analysis alone, due to the 11 m flight path, because the energy resolution would be too poor. However, it is possible to distinguish a clear difference between measurements with and without the scattering foil. The peaks in the background measurement (no target) are almost symmetric in ToF, centered at a ToF compatible with γ-rays. For this reason, this background is called *γ-flash*, even if it could be due to at least four processes: (1) γ-rays from the target, (2) γ-rays induced by spallation neutrons (hundreds of MeV) with a velocity not distinguishable from light, (3) charged particles (including protons) induced by spallation neutrons, and (4) charged particles (including protons) induced by γ-rays via photonuclear reactions. Among these, (3) and (4) are the most likely because they can produce a coincidence ΔE–E event, while (1) and (2) can contribute only via random coincidences.

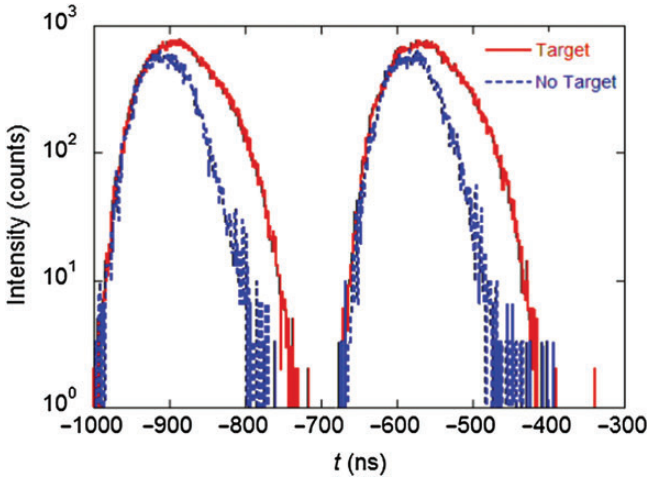

Fig. 5. Time distribution of the coincidence counts with respect to the T_0 signal of the accelerator. Comparison with a background measurement without the polyethylene target is shown.

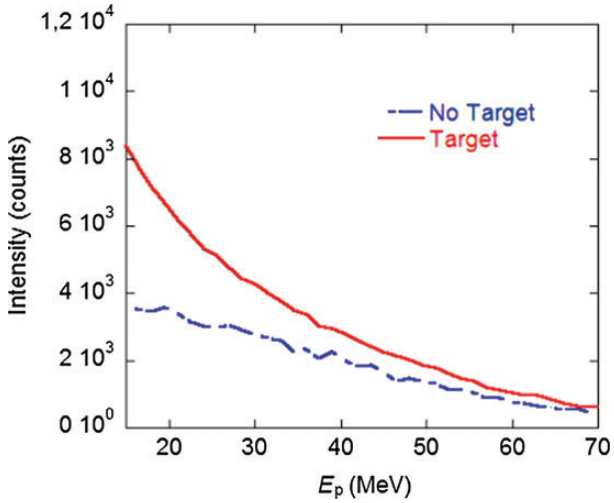

Fig. 6. Recoil proton energy distribution of the coincidence counts. Comparison with a background measurement without the polyethylene target is shown.

The ToF structures are broadened at higher ToF when the scattering target is present. These events are compatible with proton recoil of fast neutrons with energy $20\,\text{MeV} < E_n < 120\,\text{MeV}$.

In the PH spectrum, shown in Fig. 6, it is possible to notice that the normalized intensity almost doubles with the presence of the target, and the slope of the spectrum is different. The proton energy is defined as $\Delta E + E$.

5. Monte Carlo simulations

An Monte Carlo N-Particle eXtended transport code (MCNPX) model of the TPR spectrometer was used for interpretation of the measurements. In this model, the polyethylene target is included and protons are tallied by a detector at 45° with respect to the neutron-collimated beam. The effect of air is also included in the model. The neutron beam impinging on the target has a radius of 2.33 cm; the fast-neutron profile was taken from Ref. [14].

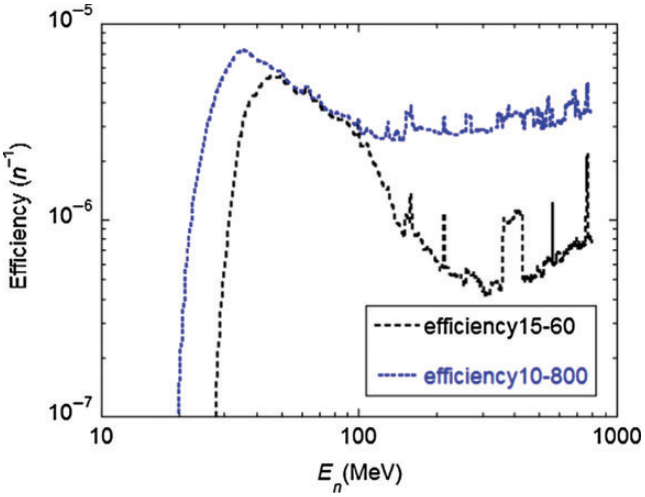

Fig. 7. MCNP simulation of the proton recoil counting efficiency for different lower and upper thresholds.

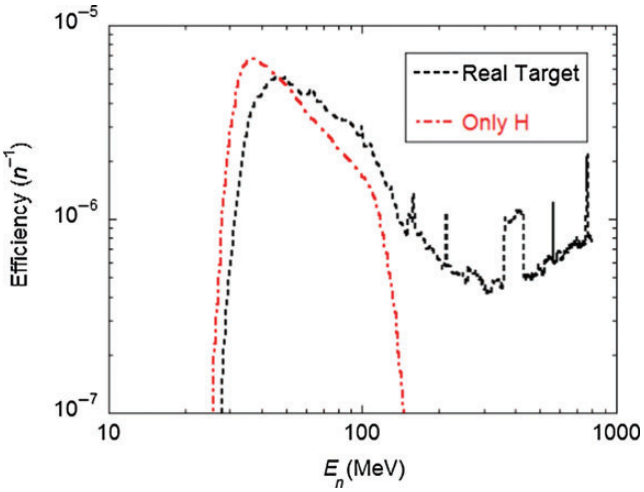

Fig. 8. MCNP simulation of the proton recoil counting efficiency for a CH_2 target in air, compared with the contribution of a hypothetic target of pure hydrogen in vacuum.

As shown in Ref. [21], the MCNPX model was used to calculate the efficiency and energy resolution of the TPR system as a function of the neutron energy. The efficiency $\mathrm{Eff}_{E1-E2}(E_n)$ is defined as the probability of a neutron of energy E_n producing a recoil proton in the energy bin $E_1 < E_p < E_2$. In Fig. 7, we compare the calculated $\mathrm{Eff}_{15-60}(E_n)$, which is relevant for this analysis, to $\mathrm{Eff}_{10-800}(E_n)$. The two curves almost overlap in the region $30\,\mathrm{MeV} < E_n < 100\,\mathrm{MeV}$, but differ significantly at higher energies. Focusing in particular on the $E_n > 100\,\mathrm{MeV}$ region of the $\mathrm{Eff}_{15-60}(E_n)$ curve, we can ascribe the high-energy continuum to interaction on carbon, with sharp peaks sitting on top of the continuum that we identify as neutron resonances on oxygen and nitrogen. For comparison, we have also run a simulation for the hypothetical case of a target of pure hydrogen in vacuum, which is compared to the real case of a polyethylene target in air in Fig. 8. The corresponding expected spectrum for the two cases, assuming a beam of 100 MeV neutrons impinging on the target, is shown in Fig. 9. Again, we note that, in the case of a real CH_2 target, the well defined peak due to elastic scattering on hydrogen is accompanied by a high-energy continuum at a level of about 10^{-1} compared to the elastic peak height and due to neutron interaction on carbon.

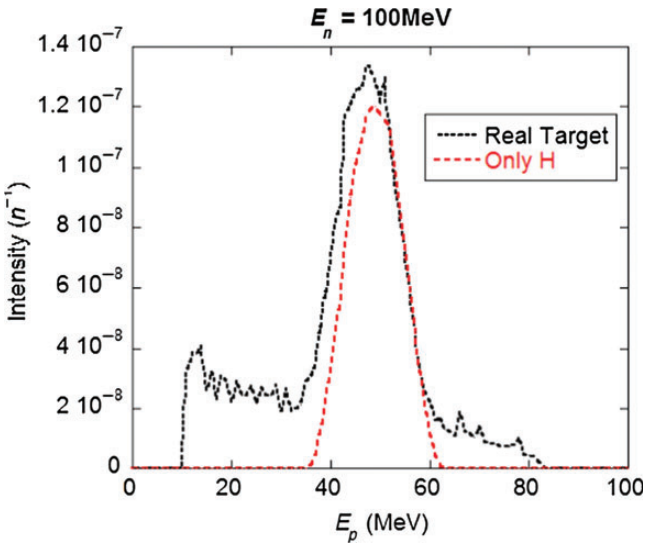

Fig. 9. MCNP simulation of the proton recoil spectrum at the detectors for an impinging beam of 100 MeV neutrons on a CH_2 target in air (black line). The expected spectrum evaluated for the case of a pure hydrogen target is also shown for comparison (red curve).

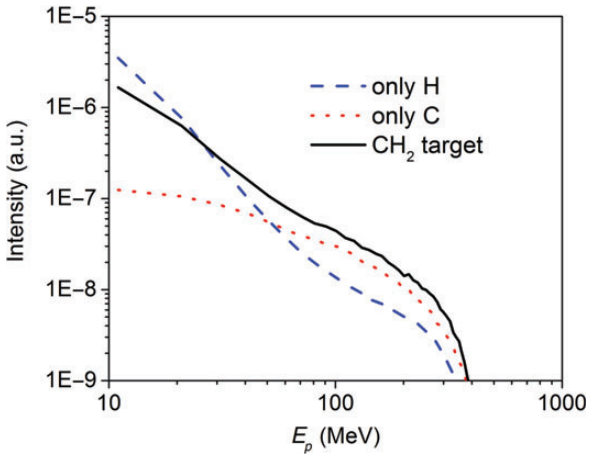

Fig. 10. MCNP simulation of the proton recoil spectrum for a CH_2 target (solid line), compared with the cases of pure hydrogen (blue dashed) and pure carbon (red dotted) targets.

The same MCNP model was then used to calculate the response to more complex white neutron spectra. The first calculation (*Simulation 1*) was performed using as input the neutron spectrum calculated for the VESUVIO beam-line, shown in Refs. [10,14]. The second calculation (*Simulation 2*) took as input a neutron spectrum with an intensity assumed to be proportional to $1/E_n$. This simplification comes from the common convention of approximating the intensity of epithermal neutron spectra from spallation sources as proportional to $1/E_n^{\alpha}$ with $\alpha \approx 1$ [7], which we have tacitly assumed to also hold at higher energies in the absence of more detailed information.

The resulting proton spectra at the detector position are shown in Fig. 10 for the *Simulation 2* scenario, where the real case of a polyethylene (CH_2) target is compared to a hypothetical case where the target is made either of hydrogen only, or of carbon, assuming a relative nuclei fraction of 1:2 as in CH_2. This was done in order to estimate the contribution of carbon to proton emission due to all the different $^{12}C(n,px)$ reaction channels [40]. One can notice from Fig. 10 that the contribution

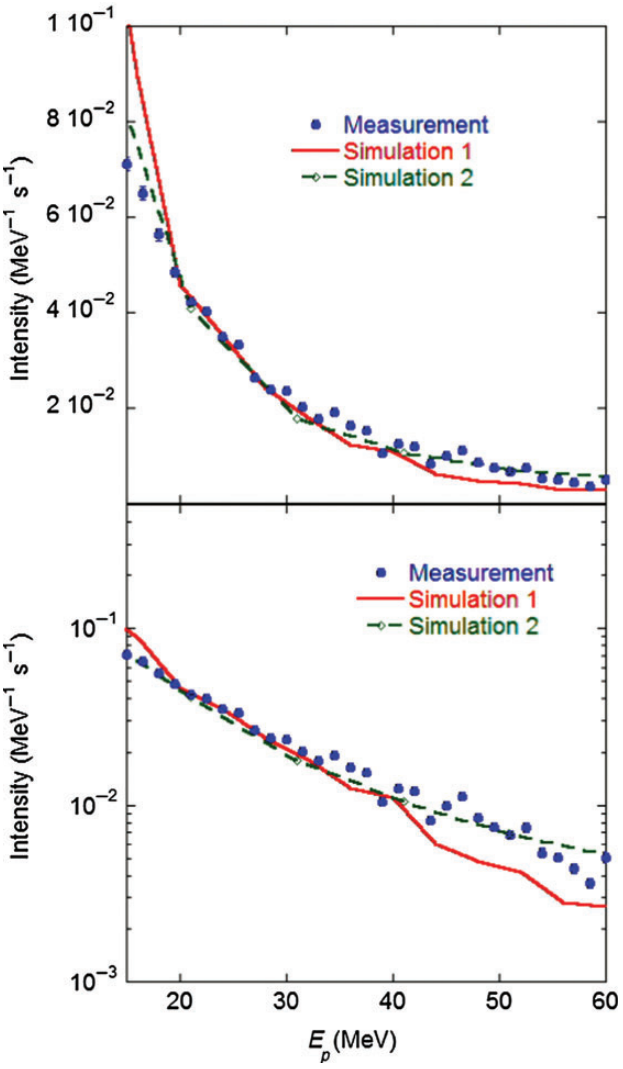

Fig. 11. Proton recoil spectrum measured by the TPR compared to Monte Carlo simulation of the VESUVIO beam-line. Linear scale is on the top, log scale on the bottom.

of elastic scattering on hydrogen dominates in the proton energy range $E_p < 50$ MeV [41], which corresponds to $E_n < 100$ MeV. In this region, the contribution of neutron inelastic scattering on carbon is below 10%. The latter becomes, however, the main contribution to proton production at higher energies, i.e. $E_p > 50$ MeV.

It is also worth noticing that proton emission from a CH_2 target cannot be obtained by summing the results for the pure proton and pure carbon targets. Other effects come into play, such as self-shielding of the target.

6. Data analysis

The simulated proton spectrum for a CH_2 target is compared to measurements in Fig. 11, showing an overall good agreement. Here the proton background contribution ("*no target*" curve in Fig. 6) has been subtracted. The simulation is normalized to a measurement using intensity as the only fit parameter.

From the combination of the measured and simulated recoil proton spectra, we can calculate the neutron flux at energies $E_n > 10\,\text{MeV}$ ($\Phi_{E_n} > 10\,\text{MeV}$) using its proportionality to the measured counting rate N_{15-60} in the $15\,\text{MeV} < E_p < 60\,\text{MeV}$ energy window, as given by

$$N_{15-60} = A \cdot \Phi_{E_n > 10\,\text{MeV}} \int_{10\,\text{MeV}}^{800\,\text{MeV}} \phi(E_n) \cdot \text{Eff}_{15-60}(E_n)\, dE_n, \tag{1}$$

where A is the area of the beam impinging on the target, and $\phi(E_n)$ is the neutron energy distribution normalized to unity in the $10 < E_n < 800\,\text{MeV}$ energy interval, i.e.

$$\int_{10\,\text{MeV}}^{800\,\text{MeV}} \phi(E_n) dE_n = 1. \tag{2}$$

From the MCNP calculation shown in Fig. 7, the integral in Eq. 1 can be computed for the "*Simulation 2*" case as

$$\int_{10\,\text{MeV}}^{800\,\text{MeV}} \phi(E_n) \cdot \text{Eff}_{15-60}(E_n)\, dE_n = 1.4363 \cdot 10^{-6}. \tag{3}$$

The measured value for N_{15-60} is (1.01 ± 0.1) cps, considering an average proton current of 160 μA. The estimated error of 10% comes from uncertainties in the extrapolation of the energy calibration of the proton spectrometer from low (a few MeV) to high energies (dozens of MeV) [27]. Future measurements at a proton accelerator providing higher proton energies than those used so far to calibrate our instrument may lower this error.

The area of the beam impinging on the target, A, is $17.05\,\text{cm}^2$ for a beam of radius $R = 2.33\,\text{cm}$. This value is taken from Fig. 11 of Ref. [14], and in particular from the curve corresponding to neutrons with deposited energy $E_d > 15\,\text{MeV}$. Here we have further assumed a homogeneous beam of $R = \text{FWHM}/2$.

A final correction to be applied comes from the fact that our measurement was carried out at the back of the irradiation table (see Fig. 1), i.e. 13 m from the spallation target, and not in the center of the beam-line tank, which sits 11.05 m from the same spallation target. The measured scaling curve from Ref. [10] suggests that a reduction by a factor of 1.94 in the neutron flux may be expected at our experimental position.

After including this correction and normalizing to a 180 μA proton current, we obtain a value of

$$\Phi_{E_n > 10\,\text{MeV}} = (8.8 \pm 0.8) \cdot 10^4\,\text{s}^{-1}\,\text{cm}^{-2}. \tag{4}$$

Table 1 compares this result to values obtained with other measurement techniques and retrieved from the literature. Our evaluation of the neutron flux based on TPR measurements is compatible within 2σ with all the others. A typical uncertainty level that can be assumed for these neutron flux evaluations is of the order of 10%, due to the known difficulties of performing neutron spectroscopy measurements at these energies. Furthermore, the reliability of the simulations may also be affected by simplifications in the geometry layout (e.g. components of the beam-line not included in the MCNP model) and, more importantly, by lack of well established nuclear cross-section data at high energies (ideally, cross sections up to 800 MeV would be needed).

Finally, against expectations, we may note that there seems to be a less robust agreement between measurements and simulations at proton energies below $E_p = 20\,\text{MeV}$, which appears to be more pronounced as the proton energy decreases. This feature is, at present, not completely understood and needs further investigation.

When comparing the results of Table 1, one should also remember that, in the absence of beam profile measurements, no divergence effect was considered when the beam travels from the center of

Table 1. Measured values of the VESUVIO neutron flux for $E_n > 10\,\text{MeV}$ at 180 μA proton current. The TPR measurement is compared to reference values from the literature.

Measurement	Flux ($s^{-1}\,cm^{-2}$)	Reference
Activation foils	$(5.8 \pm 1) \cdot 10^4$	Andreani et al. (2008) [7]
Bonner spheres	$(8.3 \pm 0.8) \cdot 10^4$	Bedogni et al. (2009) [9]
Breakdown counters	$(8.5 \pm 1) \cdot 10^4$	Smirnov et al. (2012) [10]
Telescope proton recoil	$(8.8 \pm 0.8) \cdot 10^4$	This work (2015)

the beam-line to the back of the irradiation table (i.e. from 11 to 13 m). Moreover, fluxes quoted in the table using different detection techniques must be regarded as values averaged over the detector area, which may be different for the different instruments. For example, TPR and Bonner spheres have a larger detection volume than breakdown counters or activation foils, which may introduce differences if beam profile effects are important. On the other hand, the fact that quite different techniques give very similar results provides extra confidence in the reliability of the numbers found.

7. Conclusions

A telescope proton recoil spectrometer was optimized for fast-neutron measurements at pulsed spallation sources. Good background discrimination was obtained with the present detector configuration, using in coincidence a 500 μm silicon detector and a 2.5 cm thick YAP scintillator. Recoil proton measurements at the VESUVIO beam-line are presented in the $15\,\text{MeV} < E_p < 60\,\text{MeV}$ energy range. Monte Carlo simulations of the VESUVIO beam-line are used for analysis of the experimental data. The neutron flux for $E_n > 10\,\text{MeV}$ was found to be $(8.8 \pm 0.8) \cdot 10^4\,\text{cm}^{-2}\,\text{s}^{-1}$ at 180 μA proton current.

References

[1] C. D. Frost, S. Ansell, and G. Gorini, A new dedicated neutron facility for accelerated SEE testing at the ISIS facility. In *Reliability Physics Symposium, 2009 IEEE International* (IEEE, 2009), pp. 952–955.
[2] M. S. Gordon et al., IEEE Trans. Nucl. Sci. **51**, 3427 (2004).
[3] E. Normand, IEEE Trans. Nucl. Sci. **43**, 2742 (1996).
[4] A. Taber and E. Normand, IEEE Trans. Nucl. Sci. **40**, 120 (1993).
[5] P. E. Dodd and L. W. Massengill, IEEE Trans. Nucl. Sci. **50**, 583 (2003).
[6] J. F. Ziegler, IBM J. Res. Dev. **40**, 19 (1996).
[7] C. Andreani et al., Appl. Phys. Lett. **92**, 114101 (2008).
[8] S. Platt et al., IEEE Trans. Nucl. Sci. **55**, 2126 (2008).
[9] R. Bedogni et al., Nucl. Instrum. Meth. A **612**, 143 (2009).
[10] A. N. Smirnov et al., Nucl. Instrum. Meth. A **687**, 14 (2012).
[11] A. Pietropaolo et al., Europhys. Lett. **92**, 68003 (2010).
[12] A. Pietropaolo et al., Europhys. Lett. **94**, 62001 (2011).
[13] M. Rebai et al., Nucl. Phys. B Proc. Suppl. **215**, 313 (2011).
[14] M. Rebai et al., J. Instrum. **7**, C05015 (2012).
[15] C. Cazzaniga et al., Rev. Sci. Instrum. **85**, 11E101 (2014).
[16] C. Cazzaniga et al., Rev. Sci. Instrum. **85**, 043506 (2014).
[17] F. Murtas et al., J. Instrum. **7**, P07021 (2012).
[18] G. Croci et al., Nucl. Instrum. Meth. A **720**, 144 (2013).
[19] G. Croci et al., J. Instrum. **7**, C03010 (2012).
[20] G. Croci et al., J. Instrum. **8**, P04006 (2013).
[21] S. P. Platt, A. V. Prokofiev, and X. Cai, Fidelity of energy spectra at neutron facilities for single-event effects testing. In *Reliability Physics Symposium (IRPS), 2010 IEEE International* (IEEE, 2010), pp. 411–416.
[22] C. Cazzaniga et al., J. Instrum. **8**, P11008 (2013).

[23] J. Blomgren, N. Olsson, and J. Rahm, Phys. Scripta **2000**, no. T87, 33 (2000).
[24] J. F. Ziegler, *SRIM—The Stopping, Range of Ions in Solids*. (Available at: http://www.srim.org/, date last accessed June 25, 2015).
[25] Hamamatsu webpage, http://www.hamamatsu.com, date last accessed June 25, 2015.
[26] CIVIDEC webpage, http://www.cividec.at, date last accessed June 25, 2015.
[27] C. Cazzaniga et al., Nucl. Instrum. Meth. A **751**, 19 (2014).
[28] A. Fazzi et al., *Nuclear Science Symposium and Medical Imaging Conference (NSS/MIC), 2013 IEEE* (IEEE, 2013), pp. 1–4.
[29] DT5751 2/4 channel 10 bit 2/1 GS/s digitizer (CAEN—Costruzioni Apparecchiature Elettroniche Nucleari S.p.A.). (Available at: http://www.caen.it/, date last accessed June 25, 2015).
[30] M. Nocente et al., Rev. Sci. Instrum. **81**, 10D321 (2010).
[31] M. Nocente et al., Nucl. Fusion **52**, 063009 (2012).
[32] M. Nocente et al., IEEE Trans. Nucl. Sci. **60**, 1408 (2013).
[33] M. Nocente et al., Rev. Sci. Instrum. **85**, 11E108 (2014).
[34] A. Pietropaolo et al., Nucl. Instrum. Meth. A **568**, 826 (2006).
[35] A. Pietropaolo et al., Nucl. Instrum. Meth. A **608**, 121 (2009).
[36] C. Cazzaniga et al., Rev. Sci. Instrum. **84**, 123505 (2013).
[37] C. Cazzaniga, M. Nocente, M. Tardocchi, M. Rebai, M. Pillon, F. Camera, A. Giaz, L. Pellegri, and G. Gorini, Nucl. Instrum. Meth. A **778**, 20 (2015).
[38] C. Cazzaniga et al., Nucl. Instrum. Meth. A **732**, 384 (2013).
[39] M. S. Livingston and H. A. Bethe, Rev. Mod. Phys. **9**, 285 (1937).
[40] I. Slypen, V. Corcalciuc, and J.-P. Meulders, Phys. Rev. C **51**, 1303 (1995).
[41] S. Chiba, S.-i. Morioka, and T. Fukahori, J. Nucl. Sci. Technol. **33**, 654 (1996).